Application and assessment of a membrane-based pCO_2 sensor under field and laboratory conditions

Zong-Pei Jiang*[1,2], David J. Hydes[1], Sue E. Hartman[1], Mark C. Hartman[1], Jon M. Campbell[1], Bruce D. Johnson[3], Bryan Schofield[3], Daniela Turk[4,5], Douglas Wallace[4], William Burt[4], Helmuth Thomas[4], Cathy Cosca[6], Richard Feely[6]

[1] National Oceanography Centre Southampton, European Way, Southampton, UK

[2] State Key Laboratory of Marine Environmental Science, Xiamen University, Xiamen, China

[3] ProOceanus Systems Inc., Bridgewater, Nova Scotia, Canada.

[4] Department of Oceanography, Dalhousie University, Halifax, NS, Canada

[5] Lamont-Doherty Earth Observatory, Columbia University, NY, USA

[6] Pacific Marine Environmental Lab, NOAA, Seattle, WA, USA

*Corresponding author: Zong-Pei Jiang

National Oceanography Centre Southampton, University of Southampton

European Way, Southampton, United Kingdom, SO14 3ZH

Running head: Assessment of a membrane-based NDIR pCO_2 sensor

Acknowledgment

The Swire Charitable Trust and the Swire Education Trust are gratefully acknowledged for funding the Swire NOCS Ocean Monitoring System (SNOMS) project and the scholarship for Zong-Pei Jiang's PhD study. The Swire Group Company China Navigation and the crews on the *MV Pacific Celebes* are to be thanked for supporting the operation of the SNOMS project. Dave Childs provided invaluable analysis of the salinity samples at NOCS. At the Institute of Ocean Science in Canada, Marty Davelaar, Jim Christian and Kyle Davidson helped with sample pickups and joined in the SNOMS sample processing exercise. We gratefully thank Jim Eddington, Emily Chua, Claire Normandeau, Trina Whitsitt and Douglas Schillinger during the Aquatron tests at Dalhousie University. We also thank the support from Richard Lampitt, Kate Larkin, Maureen Pagnani, Thanos Gkritzalis on the sensor deployment and maintenance at the PAP site. Wei-Jun Cai is thanked for the helpful discussion on the organic alkalinity. We also thank Mike DeGrandpre and Wiley Evans for their helpful suggestions on improving this paper.

Abstract

The principle, application and assessment of the membrane-based ProOceanus CO_2-Pro^{TM} sensor for partial pressure of CO_2 (pCO_2) are presented. The performance of the sensor is evaluated extensively under field and laboratory conditions by comparing the sensor outputs with references of direct measurements from calibrated pCO_2 measuring systems and the thermodynamic carbonate calculation from discrete samples. Under stable laboratory condition, the sensor agreed with a calibrated water-air equilibrator system at -3.0 ± 4.4 μatm during a 2-month intercomparison experiment. When applied in field deployments, the larger differences between measurements and the calculated pCO_2 references (6.4 ± 12.3 μatm on a ship of opportunity and 8.7 ± 14.1 μatm on a mooring) are related not only to sensor error, but also to the uncertainties of the references and the comparison process, as well as changes in the working environments of the sensor. When corrected against references, the overall uncertainties of the sensor results are largely determined by those of the pCO_2 references (± 2 and ± 8 μatm for direct measurements and calculated pCO_2 respectively). Our study suggests accuracy of the sensor can be affected by temperature fluctuations of the detector optical cell and calibration error. These problems have been addressed in more recent models of the instrument through improving detector temperature control and through using more accurate standard gases. Another interesting result in our laboratory test is the unexpected change in alkalinity which results in significant underestimation in the pCO_2 calculation as compared to the direct measurement (up to 90 μatm).

Introduction

The knowledge of surface ocean CO_2 variability is important for understanding the marine carbon cycle and its future response to the absorption of anthropogenic CO_2 (Doney et al. 2009). In the past few decades, high-accuracy seawater pCO_2 measuring systems (Körtzinger et al. 1996; Dickson et al. 2007; Pierrot et al. 2009) have been widely used on research vessels providing high quality pCO_2 data, which leads to the generation of a global atlas of the surface ocean pCO_2 (Surface Ocean CO_2 Atlas, http://www.socat.info/, Bakker et al. 2013) and CO_2 flux (Takahashi et al. 2009). However, there is still a lack of data from large areas of the globe, especially in the shelf seas, Southern Ocean, and southern-hemisphere subtropical gyres (Doney et al. 2009). Moreover, changes in seawater pCO_2 can occur on timescales from daily (Degrandpre et al. 1998; Yates et al. 2007; Dai et al. 2009; Turk et al. 2013) to seasonal and interannual (Bates 2002, 2007; Watson et al. 2009; Jiang et al. 2013), especially in the dynamic coastal environments (Borges and Frankignoulle 1999; Thomas and Schneider 1999; De La Paz et al. 2008; Turk et al. 2010; Jiang et al. 2011). Observations with sufficient temporal and spatial resolution are thus needed for a better understanding of the controlling mechanism of pCO_2 variability in different regions and for a more reliable CO_2 flux estimation.

In addition to the traditional shipboard measuring system (e. g. the General Oceanics pCO_2 measuring system) , there are emerging techniques to develop autonomous pCO_2 sensors. As summarized in Table 1, these sensors generally follow the same basic concept based on the measurement of a gas or indicator solution that is in equilibrium with the seawater to be determined. The equilibrium state can be reached by using water-gas equilibrators where the gas is directly in contact with the seawater, or via gas permeable interfaces such as polydimethylsiloxane

(PDMS) or polytetrafluoroethene (PTFE) membrane. The equilibrated gas can be measured by a non-dispersive infrared (NDIR) spectrometry, while the equilibrated indicator solution can be determined by electrode, fluorescence or spectrophotometric methods (Table 1). For these reagent-based fibre optic chemical sensors (Goyet et al. 1992; Degrandpre 1993; Lefévre et al. 1993; Degrandpre et al. 1995), improvements have been made by using multi-wavelength detection and long pathlength liquid-core waveguides for better precision and accuracy (Degrandpre et al. 1999; Wang et al. 2002; Wang et al. 2003; Nakano et al. 2006; Lu et al. 2008). Evolving sensor technology has enabled cost-effective pCO_2 measurements to be made on various platforms such as ship of opportunity (SOO), buoy and mooring, glider, profiling float and autonomous underwater vehicle (Degrandpre et al. 1998; Nakano et al. 2006; Nemoto et al. 2009; Willcox et al. 2009; Fiedler et al. 2012; Saderne et al. 2013).

In this paper, we describe the principle and design of a membrane-based NDIR pCO_2 sensor (ProOceanus CO_2-Pro^{TM}, hereafter referred to as CO_2-Pro). The sensor's functionality, reliability and accuracy are evaluated under various situations including: a 16-day coastal mooring deployment test adjacent to a coral reef in Hawaii (October to November 2009), shipboard underway mapping on a SOO (October 2009 to March 2012), intercomparison with a calibrated water-gas equilibrator system in the Aquatron Laboratory at Dalhousie University (May to September 2012) and long-term open-ocean mooring deployment in the Northeast Atlantic (June 2010 to July 2012). The performance of the CO_2-Pro is assessed by comparing the sensor outputs against two kinds of reference: (1) the thermodynamic carbonate calculation of pCO_2 from the determinations of dissolved inorganic carbon (DIC), total alkalinity (TA), and pH from discrete samples; (2) direct measurements by the traditional water-gas equilibrator NDIR systems which

97 are regularly calibrated against standard gases. The advantages and limitations of the CO_2-Pro are
98 summarized and the recent improvements of the instrument are introduced.

99 **Materials and Procedures**

100 ***Principle of the CO_2-Pro***

101 The CO_2-Pro is designed as a light-weight, compact, plug and play, versatile instrument for pCO_2
102 measurements on moorings, drifters and profilers, in underway mode and in laboratories. As
103 shown in Figure 1, the sensor is fitted with an equilibrator composed of a gas permeable PDMS
104 membrane (other membrane materials are also available) and an internal detection loop with a
105 NDIR detector based on a highly modified PPSystems SBA-4 CO_2 analyzer. The patented gas
106 transfer interface of the equilibrator features a tubular design, through which the equilibration
107 between the surrounding water and the internal gas stream can be achieved. Copper wire is wound
108 round the tube to inhibit the potential for bio-film formation and the equilibrator is protected from
109 physical damage by an end-cap. An associated Seabird Electronics SBE 5M submersible pump
110 flows water past the outer surface of the equilibrator membrane to accelerate the equilibration.
111 The response time, i.e. the time for the membrane to reduce the perturbation in pCO_2 by a factor
112 of 1/e, is typically 2 minutes depending on the pumping rate. NDIR measurement on the
113 equilibrated internal gas is taken at a wavelength of 4.26 μm at a controlled optical cell
114 temperature (30, 40 or 55°C). In addition, temperature, pressure and humidity of the internal gas
115 are determined to correct the CO_2 measurement. Further detailed specifications of the CO_2-Pro can
116 be found at the company's website http://www.pro-oceanus.com/co2-pro.php.
117 When the sensor is turned on, the optical cell of the detector warms up and then stabilizes at the
118 temperature set point. A zero point calibration (ZPC) is then carried out to provide a zero-CO_2

baseline (C_{zero}) for the subsequent NDIR absorption measurement. This is done by circulating the internal gas through a CO_2 absorption chamber containing soda lime or Ascarite (flow path: valve 2 - circulation pump - optical cell - valve 3 - absorption chamber - valve 2, Fig. 1). When the ZPC finishes, the solenoid valves 2 and 3 are activated to circulate the internal gas around a closed circuit connecting the equilibrator and detector (flow path: valve 2 - circulation pump - optical cell - valve 3 - valve 4 - equilibrator - valve 1- valve 2, Fig. 1). The inferred signal of the internal gas (C_{meas}) is measured to calculate the absorbance ($\varepsilon = C_{meas}/ C_{zero}$) and CO_2 concentration. Once the internal gas is equilibrated with the water surrounding the equilibrator (typically 10-15 minutes after the ZPC), the seawater CO_2 concentration can be determined. The CO_2-Pro features a programmable regular automatic ZPC function to correct the detector drift which can be caused by contamination of the optical cell, optical source ageing and changes in detector sensitivity.

Each CO_2-Pro is factory calibrated at a known optical cell temperature and pressure against 5 standard gasses with xCO_2 (mole fraction of CO_2 in dry air) spanning from 0 to 600 ppm (other calibration ranges are also available). The calibration equation is obtained by a three-segment least-squares fitting to a quadratic equation between ε and xCO_2. This equation is subsequently tested by measuring a further three known mixtures of CO_2. While the calibration equation provides a raw xCO_2 from the inferred measurement, empirical corrections are applied to account for the differences of conditions between calibration and measurement (temperature, pressure, water vapour). As the actual measurement is made on gas which is nearly saturated with water vapour, the output of CO_2-Pro is the mole fraction of CO_2 in wet air (wCO_2, ppm) and pCO_2 in the measured water is obtained by: $pCO_2 = wCO_2 * P_{wet}$, where P_{wet} is the measured total pressure of the internal gas which includes water vapour pressure.

ACT coastal mooring test

The application of the CO_2-Pro in coastal mooring measurement was previously tested in a demonstration project organized by the Alliance for Coastal Technologies (ACT) (http://www.act-us.info/evaluations.php#pco2). During October to November 2009, a CO_2-Pro was mounted on a surface mooring and deployed at a fixed depth of 1 m close to a shallow sub-tropical coral reef in Kaneohe Bay, Hawaii. Continual measurements were made by the CO_2-Pro on an hourly basis and the results were compared with the reference pCO_2 calculated from discrete samples. pH and TA of these samples were measured spectrophotometrically using meta-cresol purple and bromo-cresol green as indicators, respectively (Dickson et al. 2007). Both measurements were calibrated against the Certified Reference Material (CRM) from Scripps Institution of Oceanography. The accuracy of the pH measurement was estimated to be 0.005 and the standard deviation (SD) of repeated TA measurements was 1.9 μmol kg^{-1} (ACT 2009b). Details of the deployment, measurements, calculation and quality control were documented by ACT (2009a, b).

SNOMS underway measurements

From June 2007 to March 2012, CO_2-Pro sensors were used for continuous shipboard underway measurement in the operation of a SOO-based measuring system (referred to as SNOMS) on the *MV Pacific Celebes* (Hydes et al. 2013). For these measurements a CO_2-Pro was mounted in a 45-litre flow-through pressure tank, together with other sensors for temperature, conductivity, dissolved oxygen and total dissolved gas pressure. To adapt it to the SNOMS tank, the protecting end-cap and the associated water pump of the CO_2-Pro were removed. The gas transfer interface was thus directly exposed to the seawater for pCO_2 measurement, which also enabled direct

cleaning of the membrane surface. The SNOMS tank was fed at a flow rate of 28 ± 2 litres minute^{-1} by a branch of the non-toxic seawater being pumped to the ship's fresh water generator. This water supply was routinely turned off in shallow and potentially turbid water, thereby preventing sedimentation in the tank and contamination of the membrane of the CO_2-Pro. At each port, the tank was opened and the CO_2-Pro membrane was cleaned by hosing it down with fresh water.

The CO_2-Pro was continuously working when the SNOMS system was in operation. The frequency of the automatic ZPC was set to be 6 hours, and the 15 minutes of data after each ZPC (when the internal gas was re-equilibrating with the water) was discarded. In order to account for the difference between the water temperature in the tank (T_{tank}) and that in the surface ocean, an insulated Seabird 48 hull-contact temperature sensor was used to monitor the sea surface temperature (SST). The time lag between SST and T_{tank} was estimated to be ~30 seconds. By considering the temperature effect on pCO_2 (Takahashi et al. 1993), the tank water pCO_2 measured by CO_2-Pro ($pCO_{2,Pro}$) was corrected to the sea surface condition: $pCO_{2,SST} = pCO_{2,Pro} * \exp[0.0423* (SST-T_{tank})]$ The likely accuracy of SST from the hull measurement is 0.1 °C (Beggs et al. 2012), which results in an uncertainty of ~1.5 μatm in converting $pCO_{2,Pro}$ to $pCO_{2,SST}$.

In addition to the underway measurements, discrete samples were collected by the ship's engineers for the determination of DIC and TA. These samples were shipped to the National Oceanography Centre, Southampton (NOCS) and were measured under stable laboratory conditions. The CRM-calibrated measurements of DIC and TA were carried out using a VINDTA 3C (Marianda, Germany). Repeat measurements on pooled samples were undertaken before

sample analysis each day (n>3), these suggested a precision better than ± 2 μmol kg^{-1} for DIC and ± 1.5 μmol kg^{-1} for TA respectively.

The Aquatron laboratory test

After the operation on the *MV Pacific Celebes*, a controlled test of the CO_2-Pro as a part of the SNOMS tank was carried out in the Aquatron Laboratory at Dalhousie University during May to September 2012. To carry out this test, a two cubic metre open tank (referred to as the Aquatron tank) was set up beside the SNOMS tank. The two tanks were filled with sand-bed filtered seawater pumped from an adjacent harbour (estuary) on 23 May. The water was continuously pumped in a circuit between the two tanks with a turnover time of about 2 hours. The pCO_2 of the tank water was monitored by the CO_2-Pro in the SNOMS system which operated in a similar way as on the *MV Pacific Celebes*. After a stabilization period of ~50 days when the pCO_2 reached a relatively constant range, another pCO_2 measuring system (referred to as the NOIZ system) was set up in the Aquatron tank for a side-by-side comparison with the CO_2-Pro. In order to control pCO_2 to ocean values during the two-month intercomparison exercise (13 July to 11 September), a simple system was developed to bubble CO_2-free gas (laboratory air passing through a cartridge filled with soda lime) into the Aquatron tank on three occasions (started on 10 July, 2 August and 31 August, Fig. 6).

The NOIZ system consisted of a bubble type water-gas equilibrator and a Licor 7000 NDIR detector (Körtzinger et al. 1996). The equilibrator was mounted on the Aquatron tank and its lower part was submerged in the water to minimize the temperature difference between the tank water and that in the equilibrator. The detector was calibrated every a few days with zero CO_2 concentration nitrogen gas and an air mixture calibrated with National Oceanic and Atmospheric

206 Administration (NOAA) standard gas before 27 August 2012. After that, the calibration directly
207 used a NOAA-supplied standard gas with an uncertainty of ± 1 ppm. No shift could be identified
208 in the calibration when calibration gasses were changed. The accuracy of the pCO_2 measured by
209 the NOIZ system was estimated to be within 2 μatm.
210 In additional to the pCO_2 measurements, discrete samples for DIC and TA were collected
211 throughout the test on a daily basis. Nutrient samples were collected from 5 June onwards for
212 determination of nitrate, silicate, phosphate and ammonia (Whitledge et al. 1981). To compensate
213 for water loss due to sampling and evaporation, the Aquatron tank was topped up every 4-7 day
214 with newly pumped water. Although this water was pumped from the same location, it may
215 have different properties compared to the original tank water due to the temporal variability at the
216 sampling site. However, these top up events only had a minor influence on the chemical
217 concentrations of the tank water because of the relatively small volumes added (0.2-3% of the
218 total volume of the Aquatron tank). One exception was a substantial top up on 7 August (35%
219 of the total volume) because of a large drainage from the sampling tube, which significantly
220 changed the properties of the tank water (see the results section below).
221 ***Long-term in situ operation on the PAP mooring***
222 Since June 2010, the CO_2-Pro was used for long-term in situ deployment at the Porcupine Abyssal
223 Plain site (PAP, 49 °N 16.5 °W, 4800 m water depth) which is the longest running
224 multidisciplinary observatory in the Northeast Atlantic (Hartman et al. 2012). It was deployed on a
225 sensor frame at a fixed depth of 30 m together with other autonomous sensors for temperature,
226 salinity, chlorophyll-a fluorescence and nitrate. All these sensors were controlled by a hub
227 controller which communicated with NOCS via satellite in near real-time. The CO_2-Pro was

powered by the solar panels on the mooring and its measurement frequency and the time length for each measurement could be changed remotely.

The carbonate system calculation

The marine carbonate system can be characterized from any two of the four parameters: DIC, TA, pCO_2 and pH (Zeebe and Wolf-Gladrow 2001). In this study, the Excel program "CO2SYS" (Pierrot et al. 2006) was used for the carbonate calculations. The dissociation constants of carbonic acid (pK_1 and pK_2) determined in real seawater by Millero et al. (2006) are in good agreement with previous measurements (Mehrbach et al. 1973; Mojica Prieto and Millero 2002), and are more reliable than those measured in artificial seawater (Millero et al. 2006). Therefore, we chose to use the constants of Millero et al. (2006) in our CO2SYS calculations. The sulphuric dissociation was chosen as Dickson (1990) and the total boron fomulation was selected as Lee et al. (2010). In this study, pCO_2 was calculated either from the combination of pH and TA (ACT test) or DIC and TA (SNOMS and Aquatron test). The uncertainty of the pCO_2 calculation comes from inaccuracies in the thermodynamic dissociation constants (mainly pK_1 and pK_2) and the experimental measurements of the variables used for calculation (Millero et al. 2006). As shown in Table, 2, the various sources of uncertainties associated with the carbonate calculation yield uncertainties in the calculated pCO_2 which are estimated to be ± 7.5 μatm for the ACT test (ACT 2009a, b), ± 8.1 μatm for the SNOMS operation and ± 9.9 μatm for the Aquatron test within the measured pCO_2 ranges, respectively.

Assessment

Results of the ACT coastal mooring test

The results of the ACT mooring test have been reported by ACT (2009a) and are briefly summarized here. During the 16-day continuous measurement in Kaneohe Bay, nearly 100% of the data were retrieved except for the data gaps during calibration cycles. The hourly time series data from the CO_2-Pro ($pCO_{2,Pro}$ in Fig. 2A, 280-840 μatm) shows a significantly greater dynamic range compared to the values calculated from pH and TA ($pCO_{2,pHTA}$, 314-608 μatm). The higher measurement frequency of the CO_2-Pro thus better characterized the short-term variability of pCO_2 that was mainly caused by the strong biological activities of the adjacent coral reef system. The 5-minute averages of the sensor outputs bracketing the time of discrete sample collection were compared to the calculated $pCO_{2,pHTA}$ in Figure 2. The mean and SD of the differences between the paired $pCO_{2,Pro}$ and $pCO_{2,pHTA}$ measurements ($\delta pCO_2 = pCO_{2,Pro} - pCO_{2,pHTA}$, Fig. 2C, δpCO_2 refers to the difference between the raw/corrected sensor output and the pCO_2 reference, the same hereafter) are 8.7 ± 14.1 μatm. $pCO_{2,Pro}$ shows a tight correlation with $pCO_{2,pHTA}$ (R^2 = 0.99, n = 29, not shown), and the positive correlation between δpCO_2 and $pCO_{2,Pro}$ suggests an increasing offset under high pCO_2 conditions (Fig. 2B). This indicates that the δpCO_2 may have been subject to a linear calibration error. When $pCO_{2,Pro}$ is corrected against $pCO_{2,pHTA}$, the SD of the difference between the corrected sensor output ($pCO_{2,ProCorr}$) and $pCO_{2,pHTA}$ is ± 7.4 μatm ($\delta pCO_{2,corr}$ in Fig. 2D), which is similar to the uncertainty of $pCO_{2,pHTA}$ calculation (± 7.5 μatm). There are no systematic changes in $\delta pCO_{2,corr}$ (Fig. 2D), which suggests no other significant sources of error (i.e. biofouling, instrument drift) during the measurement. While the CO_2-Pro performed very well among submersible CO_2 sensors in the study (ACT 2009a), the potential error in sensor measurement resulting from temperature fluctuation of the optical cell (see the PAP result section below) was not considered in the performance report by ACT (2009a).

Results of the SNOMS underway measurement

The CO_2-Pro units used in the SNOMS operation were factory calibrated on a yearly basis. For evaluation purposes, $pCO_{2,Pro}$ is compared to the $pCO_{2,DICTA}$ calculated from the daily DIC and TA samples, as well as to direct measurements from other pCO_2 measuring systems in the same region. As the pCO_2 measurements were intermittent at the beginning of the SNOMS project during the circumnavigation of the *MV Pacific Celebes* (2007-2009), the assessment presented below is based on the continuous measurements along the repeated transects in the Pacific (2009 onwards). From October 2009 to February 2012, the cargo ship in total made 18 transects between the western US coast, New Zealand and Australia and two CO_2-Pro units were used for measurement in turn (Table 3). Of the 14 transects with successful instrumental measurements (other 2 transects failed with sensor malfunction), there are 12 transects with DIC and TA data.

The difference between the raw sensor output $pCO_{2,Pro}$ (5-minute average corresponding to the sampling time) and $pCO_{2,DICTA}$ is shown in Fig. 3A. The overall offset ($\delta pCO_2 = pCO_{2,Pro} - pCO_{2,DICTA}$) for the 12 transects is 6.4 ± 12.3 μatm (n=200). No correlation between δpCO_2 and the absolute concentration of pCO_2 (300-500 μatm) is identified (not shown). It is noted that the mean and SD of δpCO_2 vary from transect to transect (Table 3). Aside from any error and potential drift of the sensor, the difference in δpCO_2 among transects may be caused by several other factors: 1) uncertainty in the $pCO_{2,DICTA}$ calculation; 2) the different responses of the two CO_2-Pro units and the changing response of each unit before/after the recalibration in June 2010; 3) the influence of water patchiness, i.e. taking a discrete sample from a different water patch from that measured by the CO_2-Pro as the ship travelled at a relatively high speed (~15 knots). On the other hand, δpCO_2 values from successive transects using the same sensor generally do not differ

293 greatly (e.g. transects 2, 3, 4 for sensor 47 and transects 7, 8 ,9 for sensor 48, see Table 3). The
294 changes in δpCO_2 among these successive transects may be mainly related to the changes in the
295 condition of the gas transfer membranes (biofouling, contamination et al.) and the SNOMS tank
296 (sedimentation). The values of δpCO_2 show a random distribution around the mean value for each
297 transect except for transects 14 and 17 (Fig. 3C, D). The δpCO_2 in transect 14 shows a consistent
298 increasing trend with time which may be associated with the contamination of the equilibrator or
299 SNOMS tank (Fig. 3C). Moreover, values from the first 15 days of transect 17 (24.1 μatm) are
300 significantly higher than those of the adjacent transects using the same sensor (2.6 and 7.4 μatm
301 for transect 16 and 18 respectively), which is followed by a sudden decrease of ~40 μatm in
302 δpCO_2 in the last 5 days (Fig. 3D). The causes of these dramatic changes in δpCO_2 during this
303 particular transect are not well identified.
304 As the calculated $pCO_{2,DICTA}$ provides a consistent reference throughout the SNOMS operation for
305 the two CO_2-Pro units before and after recalibration, we chose to correct $pCO_{2,Pro}$ against
306 $pCO_{2,DICTA}$ for each transect individually. A time-dependent correction was applied to the transect
307 14, and the data in transect 17 are corrected in two sections as described above (Fig. 3C, D). As
308 shown in Figure 3B, the SD of the differences between the corrected sensor outputs and
309 $pCO_{2,DICTA}$ is ± 7.8 μatm (Fig. 3B), which is similar to the uncertainty of the calculation of
310 $pCO_{2,DICTA}$ (± 8.1 μatm).
311 During the same period of the SNOMS transect 9, another SOO *MV Natalie Schulte* took pCO_2
312 measurement along the same route to that of the *MV Pacific Celebes*, but in a different direction
313 (Fig. 4A). The pCO_2 measuring system was operated by Pacific Marine Environmental Laboratory
314 (PMEL), which features a showerhead design of equilibrator and NDIR detection of dried gas

315 (Pierrot et al. 2009). The availability of the regularly calibrated PMEL measurements (accuracy
316 within 2 μatm) provided an opportunity for an intercomparison to evaluate the corrected SNOMS
317 pCO_2 data. As shown in Figure 4, the temperature, salinity and pCO_2 measured by the two
318 systems generally display the same latitudinal distributions. The elevated pCO_2 observed around
319 the equator suggests the influence of westward advected CO_2-rich water originating from the
320 equatorial upwelling (Fig. 4D). However, the difference in measuring time at the same location for
321 the two ships ranges 0-16 days (ΔTime in Fig. 4). Therefore, the difference of the two pCO_2
322 measurements (Fig. 4F) includes not only the errors of the two measurements but also the natural
323 spatial and temporal variability of pCO_2. The latter is related to water movement and
324 warming/cooling of the surface water, which is indicated by the temperature and salinity
325 differences between the two datasets (Fig. 4E).
326 In order to minimize the influence of natural pCO_2 variability on the comparison, the simultaneous
327 measurements by the two systems were highlighted in Figure 5. These measurements, with a time
328 difference less than 0.5 day, were made in the equatorial region when the two ships were within
329 250 km of each other. The results measured by the two ships generally agreed in salinity (0.14 ±
330 0.05) and temperature (0.28 ± 0.09 °C, Fig. 5A). Previous time-series and Lagrangian
331 observations in the equatorial Pacific show a diurnal pCO_2 variability of 2-8 μatm, which is
332 mainly controlled by the temperature fluctuation (Goyet and Peltzer 1997; Degrandpre et al. 2004).
333 In order to remove the temperature effect from the pCO_2 comparison, we normalize the $pCO_{2,Pro}$ to
334 the temperature measured by the PMEL system. When the temperature effect is removed, the
335 SNOMS pCO_2 values agree well with the PMEL measurements at -0.3 ± 3.9 μatm (δpCO_2 in Fig.
336 5B). This indicates reasonably good accuracy of the corrected SNOMS pCO_2 data (note that the

337 raw CO_2-Pro outputs have been corrected against the carbonate calculation by 8.7 μatm, see Table
338 3).

339 ***Results of the Aquatron laboratory test***

340 As shown in Fig. 6A, the water temperature during the Aquatron test generally showed a diurnal
341 variability of 1-3°C and it varied within 15.5-17.5°C during the intercomparison period (Fig. 6A).
342 The evaporation-induced increase in salinity was clearly observed and a sharp salinity drop on 7
343 August indicates the substantial addition of the fresher harbour water after drainage from the
344 sampling tube (Fig. 6B). In order to account for the changes in chemical properties due to
345 evaporation, DIC and TA are normalized to the mean salinity 32.3: nX = (X / Salinity) *32.3,
346 where X is the measured concentration of DIC or TA, and nX is the salinity-normalized
347 concentration (Fig. 6D). During the stabilization period, pCO_2 decreased from the initial value (up
348 to 900 μatm) to a relative constant range within 640-690 μatm (Fig. 6C). At the same time, DIC
349 and TA both showed an increasing trend (Fig. 6B) while the concentrations of nutrients remained
350 at low levels with little variability (Fig. 6E, F). The relatively constant nDIC (~2150 μmol kg^{-1},
351 Fig. 6D) suggests that the increase in DIC (Fig. 6B) mainly resulted from evaporation. In contrast,
352 the salinity-normalized nTA increased significantly from 2240 to 2290 μmol kg^{-1} (Fig. 6D).
353 During the intercomparison period, the pCO_2 levels were adjusted to be in the “natural” open
354 ocean range of 300-550 μatm by the bubbling of CO_2-free air (started on 10 July, 2 August and 31
355 August). Corresponding decreases in pCO_2 and DIC (Fig. 6B, C) were observed when the tank
356 was purged with CO_2-free air, which was followed by progressive increases after the bubbling
357 stopped. On 7 August, the dramatic changes in all measured variables were caused by the
358 substantial addition of newly pumped water as described above. This induced sudden decreases

359 in salinity, TA and DIC (Fig. 6A, B) that were associated with increases in pCO_2 and nutrients
360 (Fig. 6C, E, F).
361 The intercomparison of the pCO_2 measurements by the SNOMS and NOIZ systems is presented in
362 Figure 7. The CO_2-Pro functioned properly throughout the Aquatron test while the NOIZ system
363 suffered from malfunctions on a few occasions (the failed measurements are not included in the
364 intercomparison, Fig. 7A). Both measurements were averaged to 5 minute interval and $pCO_{2,NOIZ}$
365 was normalized to the temperature in the SNOMS tank to eliminate temperature influence on the
366 comparison (the average temperature difference is ~0.08 °C, which corresponds to ~1.5 μatm in
367 pCO_2). There may be a slight delay in $pCO_{2,Pro}$ when responding to the pCO_2 disturbances
368 (bubbling, water top up) as these events occurred in the Aquatron tank were first observed by the
369 NOIZ system. Overall, the pCO_2 measured by the two systems shows a tight correlation ($pCO_{2,Pro}$
370 = 0.9987 * $pCO_{2,NOIZ}$, R^2 = 0.99, not shown). The mean and SD of the differences between the
371 two measurements ($\delta pCO_2 = pCO_{2,Pro} - pCO_{2,NOIZ}$) are -3.0 ± 4.4 μatm (n = 13847, Fig. 7C).
372 δpCO_2 does not show a constant drift over the two month test (Fig. 7C) but appears to vary with
373 the absolute pCO_2 concentration (Fig. 7B), which may be due to a linear error in the sensor
374 calibration. When the CO_2-Pro measurements are calibrated against $pCO_{2,NOIZ}$, the differences
375 between the calibrated $pCO_{2,ProCorr}$ and $pCO_{2,NOIZ}$ ($\delta pCO_{2,corr}$ in Fig. 7D, 0 ± 2.9 μatm) show a
376 random distribution around the mean value throughout the intercomparison experiment, which
377 suggests no instrumental drift of the CO_2-Pro occurred during the two-month period.
378 An interesting phenomenon observed in the Aquatron test is the unexpected changes in alkalinity.
379 The increase in nTA during the stabilization period (2240 to 2290 μmol kg^{-1}, Fig. 6D) cannot be
380 explained by the changes in inorganic carbon content and nutrients: (1) the small changes in nDIC

and nutrients indicate minor TA changes resulted from biological activities such as precipitation and dissolution of $CaCO_3$ (which changes TA and DIC at a ratio of 2:1) and nutrient uptake and release by algae (which changes TA following the nutrient-H^+-compensation principle) (Wolf-Gladrow et al. 2007); (2) air-sea gas exchange of CO_2 changes DIC but does not affect the concentration of TA (Wolf-Gladrow et al. 2007); (3) the oxygen saturation varied between 86-104% (not shown) which suggests no TA changes induced by anaerobic processes. Similarly, increases in nTA observed after the top up event on 7 August (2270 to 2290 μmol kg^{-1}) also did not match the changes in nDIC and nitrates: the increasing concentrations of nDIC and nitrates during this period (Fig. 6D, E) suggests the occurrence of remineralization processes which would decrease TA.

In order to examine the TA anomaly in the Aquatron test, we calculate alkalinity from the measured DIC and pCO_2 using the CO2SYS. The calculated Alk_{sys} (uncertainty estimated to be ± 3.5 μmol kg^{-1}) is the alkalinity expected at the equilibration state of the carbonate system, which accounts for the major inorganic buffering acid-base pairs. It is shown in Figure 8A that the concentrations of Alk_{sys} are 3-24 μmol kg^{-1} lower than the measured values of TA_{meas}. This excess of TA_{meas} over the Alk_{sys} (Alk_{excess}) suggests substances or processes which affect the concentration of alkalinity and/or the titration process of alkalinity. This may be due to: waste water or reactive particles in the harbour, contamination during the pumping process, reaction with the fibreglass wall of the Aquatron tank, or the existence of organic alkalinity. Although we cannot clearly identify the source(s) of the alkalinity anomaly, it is shown that using the measured TA_{meas} for carbonate calculation would result in underestimates in pCO_2 (Fig. 8B). The $pCO_{2,DICTA}$ calculated from TA_{meas} and DIC is 7-90 μatm lower compared to the direct pCO_2 measurement,

and this underestimation ($pCO_{2,bias}$= $pCO_{2,Pro}$ - $pCO_{2,DICTA}$) shows a similar trend to that of Alk_{excess} (Fig. 8C). Closer investigation shows that the percentage bias in pCO_2 ($\%pCO_{2,bias}$= $pCO_{2,bias}$ / $pCO_{2,Pro}$) is positively correlated to the percentage bias in alkalinity ($\%Alk_{excess}$= Alk_{excess} / TA_{meas} =12.54 * $\%pCO_{2,bias}$, Fig. 8D).

Results of the long-term in situ operation on the PAP mooring

Since the first deployment in June 2010, a CO_2-Pro continuously worked at the PAP site until January 2011 when a communication cable of the hub controller broke. A calibrated unit replaced the original sensor in July 2011 and operated until March 2012 when the controlling hub was flooded. A frustratingly short deployment during May to July 2012 was due to communication failure when the sensor frame became detached from the mooring. The deployment of the CO_2-Pro at PAP was successful for up to 7 months while the failure of longer measurement was due to problems of the hub controller rather than the sensor malfunction.

In contrast to continuous measurement on SOO, the CO_2-Pro on the PAP mooring was operated intermittently (1-4 times a day) due to the limited power supply. Each measurement lasted for 45-120 minutes which assures full equilibrium with the seawater (typically within 15 minutes). The pCO_2 of the oligotrophic surface water around the PAP site is expected to show minor variability during the short duration of each measurement. However, the pCO_2 measured by the CO_2-Pro showed a consistent increase throughout each measurement (Fig. 9A presents a typical measuring cycle of the CO_2-Pro) while the in situ temperature and salinity remained unchanged (not shown). It is noted that the optical cell temperature of the detector shows an increasing trend similar to that of pCO_2 (Fig. 9A). Moreover, the cell temperature during the measurement (t_{meas}) is found to be much higher than that during the ZPC ($\Delta t_{cell} = t_{meas} - t_{ZPC}$, Fig. 9A). As the NDIR

425 measurement is affected by the optical cell temperature, this temperature fluctuation would result
426 in errors in pCO_2 detection.
427 In order to examine the influence of optical cell temperature, a laboratory test was carried out
428 when the sensor was recovered from deployment. A series of CO_2 standard gases (256, 363 and
429 459 ppm) were connected to the detector bypassing the equilibrator for direct NDIR
430 measurements. In addition, a CO_2-free gas (N_2 passing through CO_2 absorbance) was used to
431 simulate the baseline measurement of C_{zero} during the ZPC. Measurements of these gases
432 were carried out following a ZPC at 40 °C, while the temperature of the optical cell during the
433 measurement of each gas was perturbed by heating with an electric breeze and cooling with a
434 cold pack (Δt_{cell} was adjusted to be -0.7 to 1.8 °C). The test results show that the inferred
435 signals of all measured gases decrease linearly with increasing optical cell temperature (not
436 shown). As the zero-CO_2 signal also changes with temperature, using a baseline measured at
437 t_{zero} as the blank reference for measurements at different cell temperatures would result in
438 errors in calculating ε and xCO_2. As shown in Figure 9B, the errors in xCO_2 ($xCO_{2,error}$ =
439 measured xCO_2 – certified value) were linearly correlated with Δt_{cell}, and the temperature
440 effects are similar for the three standard gases at 15 ppm $°C^{-1}$. It is also shown that the errors
441 in xCO_2 can be removed if the influence of Δt_{cell} is considered in the calculations of ε and
442 xCO_2 (Fig. 9B). The scatter of the data should mainly be caused by the uneven heating or
443 cooling on the optical cell in our test.
444 When this correction of Δt_{cell} is applied to the PAP measurement, the corrected $pCO_{2,tcorr}$
445 stabilizes at 15 minutes after the ZPC as expected from the equilibrium time and shows minor
446 changes afterward (Fig. 9A). It is notable that the Δt_{cell} at the PAP mooring is quite large (up

447 to 1.5 °C), which corresponds to an error in pCO_2 as large as 25 μatm. This is because of the
448 early ZPC at low t_{ZPC} when the optical cell was not sufficiently warmed up, as well as
449 inadequate thermostat control of the optical cell, i.e. the cell temperature continued to
450 increase after the ZPC. In contrast, this issue is not significant for the continuous
451 measurements as the long-term operation allows the optical cell to be fully warmed up
452 minimizing the temperature difference between ZPC and measurement. The Δt_{cell} during the
453 SNOMS and Aquatron operations was ~ 0.2 °C corresponding to an error of 3 μatm in pCO_2;
454 corrections of Δt_{cell} are applied to the SNOMS and Aquatron data before assessment.

455 **Discussion, recommendations and improvements**

456 Overall, the CO_2-Pro is a very robust sensor suitable for onboard and in situ measurements on
457 platforms with limited working space and on platforms that cannot be serviced regularly. The
458 sensor's capacity for long-term operation is demonstrated by the successes of the SNOMS
459 operation and PAP mooring deployments. In this study, the performance of the CO_2-Pro is
460 evaluated extensively under field and laboratory conditions and the results are summarized in
461 Table 4. The CO_2-Pro agreed with a calibrated water-air equilibrator system during a 2-month
462 side-by-side laboratory intercomparison (-3.0 ± 4.4 μatm). When used at sea, the direct sensor
463 outputs differed from the calculated pCO_2 reference by 6.4 ± 12.3 μatm on a SOO and 8.7 ± 14.1
464 μatm on a mooring. These differences result from a number of factors including the uncertainties
465 in the reference and the comparison process, the sensor error, how well the sensor was set up,
466 contamination issues etc. Our study suggests that, when pCO_2 references are available for
467 correction, the uncertainty of the corrected sensor result is similar to and largely determined by the
468 uncertainties of the references.

One significant limitation of the CO_2-Pro is the lack of regular calibration against standard gases, which makes it difficult to assess the accuracy of the measurement when it is deployed alone. To remedy this potential problem, Pro-Oceanus has introduced a new version of CO_2-Pro with on-board control of a gas port for introduction of standard gases. If the CO_2-Pro is to be used for onboard or laboratory measurements, this version which enables external manual calibration is recommended to be used. In the future, an automatic calibration function using standard gases would be highly desired to optimize the accuracy of the measurement. For the field applications, users of the CO_2-Pro (and any chemical sensor that is not calibrated while deployed) should calibrate the sensor before and after long-term deployments to examine any potential drift. Collection of discrete samples over a wide range of pCO_2 concentrations for the determination of other carbonate variables is recommended to provide quality control on the sensor, and also, to provide additional information on biogeochemical variability.

Clearly, the accuracy of the calibration gases used in the original factory calibration and any subsequent recalibrations is a critical factor in sensor accuracy. However, this study reveals that some inaccuracy of the sensor may be caused by calibration error which may be related to the quality of calibration gases used. To address this problem, Pro-Oceanus has performed all factory calibrations using NOAA and NOAA traceable standard gases that are accurate to better than ±1 ppm since 2011. Moreover, our study reveals that error in pCO_2 measurement of the CO_2-Pro can result from the changes in optical cell temperature between the ZPC and measurement. This problem may be significant for the early versions of CO_2-Pro whose optical cells are not well thermostatically controlled. However, this error is correctable and can be avoided by better temperature control on the detector optical cell. Since 2011, an improved

491 temperature control is a standard feature of CO_2-Pro which stabilizes the fluctuation of the
492 temperature of the detector cell to within ± 0.05 °C.
493 In order to fulfil the target of constraining the regional air-sea CO_2 fluxes to 0.2 Pg C $year^{-1}$, pCO_2
494 measuring systems need to be accurate to within 2 μatm for seawater pCO_2 (Pierrot et al. 2009).
495 This is presently a demanding requirement for pCO_2 sensors. As demonstrated in this work, the
496 CO_2-Pro sensors that were tested (particularly the older versions) did not meet the gold standard of
497 2 μatm. However, recent improvements to the CO_2-Pro (as mentioned above) should enhance
498 sensor performance. Considering the large variability of pCO_2 in time and space, there is great
499 value in expanding in situ observations by using sensors with a known reasonably good accuracy.
500 The developing sensor technology provides a very effective way to increase the capability for
501 global and regional ocean monitoring. This can provide useful information on the surface ocean
502 where no or few measurements have been made or other extreme marine environments such as in
503 the deep ocean (the CO_2-Pro has been successfully used on the SeaCycler and NEPTUNE
504 profilers, Johnson, B personal communication) or near hydrothermal vents (Nakano et al. 2006;
505 Willcox et al. 2009). Moreover, the long-term time series data from fixed-station sensor
506 deployments provides a most powerful tool to understand the controlling mechanisms regulating
507 the changes in ocean CO_2.
508 Another interesting finding in this study is the alkalinity anomaly and the mismatch in carbonate
509 calculation in the Aquatron test. Excess of measured TA (up to 24 μmol kg^{-1}) are found in
510 comparison to that calculated from DIC and pCO_2, while the carbonate calculation of pCO_2 using
511 measured TA and DIC result in underestimation in pCO_2 (up to 90 μatm). Although the causes of
512 this TA anomaly cannot be confirmed in our study, one possible explanation is the organic

contribution to alkalinity. Many previous studies have proved the existent of organic alkalinity in both laboratory cultures (up to 800 μmol kg^{-1}) and natural coastal environments (tens of μmol kg^{-1}) (Cai et al. 1998; Hernandez-Ayon et al. 2007; Muller and Bleie 2008; Kim and Lee 2009). Since the use of alkalinity including organic bases could lead to errors in the carbonate calculation, care should be taken when making calculations for the marine carbonate system in environments with high concentration of organic matter, e.g. estuary, coastal water and incubation culture solution. When studying the organic matter-rich waters, alkalinity is recommended to be measured using method proposed by Cai et al. (1998) or Hernández-Ayón et al. (1999) to identify the organic alkalinity.

523 **Reference**

524 ACT. 2009a. Performance demonstration statement Pro-Oceanus Systems Inc. PSI CO_2-Pro^{TM}.
525 Alliance for Coastal Technologies, report Ref.No. ACT TD10-03.
526 ---. 2009b. Protocols for demonstrating the performance of in situ pCO_2 analyzers. Alliance
527 for Coastal Technologies, report Ref.No. ACT PD09-01.
528 Bakker, D. C. E. and others (2013) An update to the Surface Ocean CO_2 Atlas (SOCAT
529 version 2). Earth System Science Data Discussions, 6, 465-512,
530 doi:10.5194/essdd-6-465-2013.
531 Bates, N. R. 2002. Seasonal variability of the effect of coral reefs on seawater CO_2 and air-sea
532 CO_2 exchange. Limnol. Oceanogr. **47:** 43-52.
533 ---. 2007. Interannual variability of the oceanic CO_2 sink in the subtropical gyre of the North
534 Atlantic Ocean over the last 2 decades. J. Geophys. Res. **112:** C09013.
535 Beggs, H. M., R. Verein, G. Paltoglou, H. Kippo, and M. Underwood. 2012. Enhancing ship
536 of opportunity sea surface temperature observations in the Australian region. J. Oper.
537 Oceanogr. **5:** 59-73.
538 Borges, A. V., and M. Frankignoulle. 1999. Daily and seasonal variations of the partial
539 pressure of CO_2 in surface seawater along Belgian and southern Dutch coastal areas. J.
540 Mar. Syst. **19:** 251-266.
541 Cai, W. J., Y. C. Wang, and R. E. Hodson. 1998. Acid-base properties of dissolved organic
542 matter in the estuarine waters of Georgia, USA. Geochim. Cosmochim. Acta **62:**
543 473-483.
544 Dai, M. H. and others 2009. Diurnal variations of surface seawater pCO_2 in contrasting
545 coastal environments. Limnol. Oceanogr. **54:** 735-745.
546 De La Paz, M., A. Gomez-Parra, and J. Forja. 2008. Tidal-to-seasonal variability in the
547 parameters of the carbonate system in a shallow tidal creek influenced by
548 anthropogenic inputs, Rio San Pedro (SW Iberian Peninsula). Cont. Shelf Res. **28:**
549 1394-1404.
550 Degrandpre, M. D. 1993. Measurement of seawater pCO_2 using a renewable-reagent fiber
551 optic sensor with colorimetric detection. Anal. Chem. **65:** 331-337.
552 Degrandpre, M. D., M. M. Baehr, and T. R. Hammar. 1999. Calibration-free optical chemical
553 sensors. Anal. Chem. **71:** 1152-1159.
554 Degrandpre, M. D., T. R. Hammar, S. P. Smith, and F. L. Sayles. 1995. In situ measurements
555 of seawater pCO_2. Limnol. Oceanogr. **40:** 969-975.
556 Degrandpre, M. D., T. R. Hammar, and C. D. Wirick. 1998. Short-term pCO_2 and O_2
557 dynamics in California coastal waters. Deep Sea Res., Part II **45:** 1557-1575.
558 Degrandpre, M. D., R. Wanninkhof, W. R. Mcgillis, and P. G. Strutton. 2004. A Lagrangian
559 study of surface pCO_2 dynamics in the eastern equatorial Pacific Ocean. J. Geophys.
560 Res. **109:** C08S07.
561 Dickson, A. G. 1990. Standard potential of the ($AgCl(s)+½\ H_2(g) = Ag(s) + HCl(aq)$) cell and
562 the dissociation constant of bisulfate ion in synthetic sea water from 273.15 to 318.15
563 K. J. Chem. Thermodyn. **22:** 113-127.

564 Dickson, A. G., C. L. Sabine, and J. R. Christian (2007), *Guide to best practices for ocean*
565 *CO_2 measurements*, 191 pp., North Pacific Marine Science Organization (PICES),
566 Sidney, British Columbia.
567 Doney, S. C. and others 2009. Surface-ocean CO_2 variability and vulnerability. Deep Sea Res.,
568 Part II **56:** 504-511.
569 Fiedler, B., P. Fietzek, N. Vieira, P. Silva, H. C. Bittig, and A. Körtzinger. 2012. In situ CO_2
570 and O_2 measurements on a profiling float. J. Atmos. Oceanic Technol. **30:** 112-126.
571 Goyet, C., and E. T. Peltzer. 1997. Variation of CO_2 partial pressure in surface seawater in the
572 equatorial Pacific Ocean. Deep Sea Res., Part I **44:** 1611-1625.
573 Goyet, C., D. R. Walt, and P. G. Brewer. 1992. Development of a fiber optic sensor for
574 measurement of pCO2 in sea water: design criteria and sea trials. Deep Sea Res., Part
575 I **39:** 1015-1026.
576 Hartman, S. E. and others 2012. The Porcupine Abyssal Plain fixed-point sustained
577 observatory (PAP-SO): variations and trends from the Northeast Atlantic fixed-point
578 time-series. ICES J. Mar. Sci. **69:** 776-783.
579 Hernandez-Ayon, J. M., A. Zirino, A. G. Dickson, T. Camiro-Vargas, and E.
580 Valenzuela-Espinoza. 2007. Estimating the contribution of organic bases from
581 microalgae to the titration alkalinity in coastal seawaters. Limnol. Oceanogr. Methods
582 **5:** 225-232.
583 Hernández-Ayón, J. M. N., S. L. Belli, and A. Zirino. 1999. pH, alkalinity and total CO_2 in
584 coastal seawater by potentiometric titration with a difference derivative readout. Anal.
585 Chim. Acta **394:** 101-108.
586 Hydes, D. J. and others 2013. Report of the SNOMS Project 2006 to 2012, SNOMS: SWIRE
587 NOCS Ocean Monitoring System. Part 1: Narrative description. National
588 Oceanography Centre Research and Consultancy Report, 33.
589 Jiang, Z.-P. and others 2011. Short-term dynamics of oxygen and carbon in productive
590 nearshore shallow seawater systems off Taiwan: Observations and modeling. Limnol.
591 Oceanogr. **56:** 1832-1849.
592 Jiang, Z.-P. and others 2013. Key controls on the seasonal and interannual variations of the
593 carbonate system and air-sea CO_2 flux in the Northeast Atlantic (Bay of Biscay). J.
594 Geophys. Res. **118:** 1-16.
595 Kayanne, H. and others 2002. Submergible system to measure seawater pCO_2 on a shallow
596 sea floor. Mar. Technol. Soc. J. **36:** 23-28.
597 Kim, H.-C., and K. Lee. 2009. Significant contribution of dissolved organic matter to
598 seawater alkalinity. Geophys. Res. Lett. **36:** L20603.
599 Körtzinger, A., H. Thomas, B. Schneider, N. Gronau, L. Mintrop, and J. C. Duinker. 1996.
600 At-sea intercomparison of two newly designed underway pCO_2 systems -
601 encouraging results. Mar. Chem. **52:** 133-145.
602 Lee, S. S., C. Park, P. Fenter, N. C. Sturchio, and K. L. Nagy. 2010. Competitive adsorption
603 of strontium and fulvic acid at the muscovite–solution interface observed with
604 resonant anomalous X-ray reflectivity. Geochim. Cosmochim. Acta **74:** 1762-1776.
605 Lefévre, N., J. P. Ciabrini, G. Michard, B. Brient, M. Duchaffaut, and L. Merlivat. 1993. A
606 new optical sensor for pCO_2 measurement. Mar. Chem.**:** 189-198.

Lu, Z., M. Dai, K. Xu, J. Chen, and Y. Liao. 2008. A high precision, fast response, and low power consumption in situ optical fiber chemical pCO_2 sensor. Talanta **76:** 353-359. doi: 310.1016/j.talanta.2008.1003.1005.

Mehrbach, C., C. H. Culberson, J. E. Hawley, and R. M. Pytkowicz. 1973. Measurement of the apparent dissociation constants of carbonic acid in seawater at atmospheric pressure. Limnol. Oceanogr. **18:** 897-907.

Millero, F. J., T. B. Graham, F. Huang, H. Bustos-Serrano, and D. Pierrot. 2006. Dissociation constants of carbonic acid in seawater as a function of salinity and temperature. Mar. Chem. **100:** 80-94.

Mojica Prieto, F. J., and F. J. Millero. 2002. The values of $pK_1 + pK_2$ for the dissociation of carbonic acid in seawater. Geochim. Cosmochim. Acta **66:** 2529-2540.

Muller, F. L. L., and B. Bleie. 2008. Estimating the organic acid contribution to coastal seawater alkalinity by potentiometric titrations in a closed cell. Anal. Chim. Acta **619:** 183-191.

Nakano, Y., H. Kimoto, S. Watanabe, K. Harada, and Y. W. Watanabe. 2006. Simultaneous vertical measurements of in situ pH and CO_2 in the sea using spectrophotometric profilers. J. Oceanogr. **62:** 71-81.

Nemoto, K. and others 2009. Continuous observations of atmospheric and oceanic CO_2 using a moored buoy in the East China Sea: Variations during the passage of typhoons. Deep Sea Res., Part II **56:** 542-553.

Pierrot, D., E. Lewis, and D. W. R. Wallace. 2006. MS Excel program developed for CO_2 system calculations. ORNL/CDIAC-105a. Carbon Dioxide Information Analysis Center, Oak Ridge National Laboratory, US Department of Energy, Oak Ridge, TN.

Pierrot, D. and others 2009. Recommendations for autonomous underway pCO_2 measuring systems and data-reduction routines. Deep Sea Res., Part II **56:** 512-522.

Rubin, S. I., and H. Ping Wu. 2000. A novel fiber-optic sensor for the long-term, autonomous measurement of pCO_2 in seawater, p. 631-639 vol.631. OCEANS 2000 MTS/IEEE Conference and Exhibition.

Saderne, V., P. Fietzek, and P. M. J. Herman. 2013. Extreme Variations of pCO_2 and pH in a Macrophyte Meadow of the Baltic Sea in Summer: Evidence of the Effect of Photosynthesis and Local Upwelling. PLoS ONE **8:** e62689.

Shitashima, K. 2010. Evolution of compact electrochemical in-situ pH-pCO_2 sensor using ISFET-pH electrode, p. 1-4. OCEANS 2010.

Tabacco, M. B., M. Uttamial, M. Mcallister, and D. R. Walt. 1999. An autonomous sensor and telemetry system for low-level pCO_2 measurements in seawater. Anal. Chem. **71:** 1483-1483.

Takahashi, T., J. Olafsson, J. G. Goddard, D. W. Chipman, and S. C. Sutherland. 1993. Seasonal variation of CO_2 and nutrients in the high-latitude surface ocean: a comparative study. Global Biogeochem. Cycles **7:** 843-878.

Takahashi, T. and others 2009. Climatological mean and decadal change in surface ocean pCO_2, and net sea-air CO_2 flux over the global oceans. Deep-Sea Res., Pt II **56:** 554-577.

Thomas, H., and B. Schneider. 1999. The seasonal cycle of carbon dioxide in Baltic Sea surface waters. J. Mar. Syst. **22:** 53-67.

651 Turk, D., J. W. Book, and W. R. Mcgillis. 2013. pCO_2 and CO_2 exchange during high bora
652 winds in the Northern Adriatic. J. Mar. Syst. **117–118:** 65-71.
653 Turk, D., V. Malačič, M. D. Degrandpre, and W. R. Mcgillis. 2010. Carbon dioxide
654 variability and air-sea fluxes in the northern Adriatic Sea. J. Geophys. Res. **115:**
655 C10043.
656 Wang, Z. A., W. J. Cai, Y. C. Wang, and B. L. Upchurch. 2003. A long pathlength liquid-core
657 waveguide sensor for real-time pCO_2 measurements at sea. Mar. Chem. **84:** 73-84.
658 Wang, Z. H., Y. H. Wang, W. J. Cai, and S. Y. Liu. 2002. A long pathlength
659 spectrophotometric pCO_2 sensor using a gas-permeable liquid-core waveguide.
660 Talanta **57:** 69-80.
661 Watson, A. J. and others 2009. Tracking the variable North Atlantic sink for atmospheric CO_2.
662 Science **326:** 1391-1393.
663 Whitledge, T. E., S. C. Malloy, C. J. Patton, and C. O. Wirick. 1981. Automated nutrient
664 analysis in seawater. Brookhaven National Lab Report 51398: 216.
665 Willcox, S. and others 2009. An autonomous mobile platform for underway surface carbon
666 measurements in open-ocean and coastal waters, p. 1-8. OCEANS 2009, MTS/IEEE
667 Biloxi - Marine Technology for Our Future: Global and Local Challenges.
668 Wolf-Gladrow, D. A., R. E. Zeebe, C. Klaas, A. Kortzinger, and A. G. Dickson. 2007. Total
669 alkalinity: The explicit conservative expression and its application to biogeochemical
670 processes. Mar. Chem. **106:** 287-300.
671 Yates, K. K., C. Dufore, N. Smiley, C. Jackson, and R. B. Halley. 2007. Diurnal variation of
672 oxygen and carbonate system parameters in Tampa Bay and Florida Bay. Mar. Chem.
673 **104:** 110-124.
674 Zeebe, R. E., and D. Wolf-Gladrow (2001), *CO_2 in Seawater: Equilibrium, Kinetics, Isotopes.*,
675 356 pp., Elsevier, Amsterdam.

Table 1 The various designs of pCO_2 sensors

Equilibrator	Measured phase	Determination	References
direct contact of water-gas	gas	NDIR	ACT (2009a); Nemoto et al. (2009)
gas permeable interface	gas	NDIR	Kayanne et al. (2002); Fiedler et al. (2012); Saderne et al. (2013), this study
gas permeable interface	indicator solution	electrode	Shitashima 2010
gas permeable interface	indicator solution	fluorescence	Goyet et al. (1992); Tabacco et al. (1999); Rubin and Ping Wu (2000)
gas permeable interface	indicator solution	spectrophotometry	Degrandpre (1993); Lefévre et al. (1993); Degrandpre et al. (1995; 1999); Wang et al. (2002; 2003); Nakano et al. (2006); Lu et al. (2008)

Table 2 The estimated uncertainties of the pCO_2 (μatm) calculated from various inputs (pH and TA, or DIC and TA) in this study

	Measured pCO_2	Sources of uncertainty in pCO_2 calculation				Uncertainty of the calculated pCO_2
		pK_1, pK_2	TA	DIC	pH	
ACT	280 to 840	4 to 12	0.5		6.8	7.5
SNOMS	300 to 500	7 to 10	2.3	3.8		8.1
Aquatron	280 to 860	6 to 15	4.4	6.6		9.9

Table 3 The mean and standard deviation (SD) of the differences in the CO_2-Pro outputs ($pCO_{2,Pro}$) and those calculated from DIC and TA ($pCO_{2,DICTA}$) during the SNOMS operation in the Pacific. R^2 refer to the correlation coefficients and *n* is the number of the pairs of pCO_2.

No.	Start port	End port	Start date	End date	Sensor	$pCO_{2,Pro}$ - $pCO_{2,DICTA}$	SD	R^2	n
1	Taranga	Vancouver	23-Oct-09	11-Nov-09	48	5.7	9.8	0.91	14
2	Vancouver	Brisbane	02-Dec-09	25-Dec-09	48	failed measurement			
3	Taranga	Los Angeles	29-Jan-10	18-Feb-10	47	8.3	9.9	0.92	18
4	Los Angeles	Wellington	27-Mar-10	13-Apr-10	47	16.9	4.5	0.98	14
5	Taranga	Los Angeles	14-May-10	02-Jun-10	47	12.0	8.2	0.94	16
6	Vancouver	Auckland	25-Jun-10	14-Jul-10	48	failed measurement			
7	Taranga	Los Angeles	18-Aug-10	07-Sep-10	48	-6.6	8.6	0.97	19
8	Los Angeles	Brisbane	05-Oct-10	25-Oct-10	48	5.9	6.1	0.98	20
9	Taranga	Los Angeles	21-Nov-10	12-Dec-10	48	8.7	7.5	0.98	15
10	Los Angeles	Brisbane	18-Jan-11	12-Feb-11	none	no measurement; system removed for calibration			
11	Taranga	Los Angeles	16-Mar-11	10-Apr-11	none	no measurement; system removed for calibration			
12	Los Angeles	Brisbane	05-May-11	25-May-11	recalibrated 47	successful measurement; no DIC and TA data			
13	Taranga	Los Angeles	15-Jun-11	06-Jul-11	recalibrated 47	successful measurement; no DIC and TA data			
14	Los Angeles	Brisbane	30-Jul-11	20-Aug-11	recalibrated 47	0.3	18.0	0.85	18
15	Taranga	Los Angeles	20-Sep-11	09-Oct-11	recalibrated 47	6.6	8.3	0.94	15
16	Los Angeles	Brisbane	09-Nov-11	29-Nov-11	recalibrated 48	2.6	11.3	0.92	19
17	Taranga	Los Angeles	03-Jan-12	17-Jan-12	recalibrated 48	24.1	5.1	0.99	14
			18-Jan-12	23-Jan-12	recalibrated 48	-15.57 (sudden drop)	10.1		5
18	Los Angeles	Taranga	11-Feb-12	29-Feb-12	recalibrated 48	7.4	7.4	0.94	14

Table 4 Summary of the assessment results of the CO_2-Pro in this study

	Application	Mode	Time length	Reference and its uncertainty	Difference with the reference (μatm)	
					direct output	corrected output
ACT	mooring test	in situ	16-day	calculation from pH and TA (± 7.5 μatm)	8.7 ± 14.1	0 ± 7.4
SNOMS	SOO observation	underway	several months	calculation from DIC and TA (± 8.1 μatm)	6.4 ± 12.3	0.2 ± 7.8
				direct and calibrated measurement (± 2 μatm)		-0.3 ± 3.9
Aquatron	laboratory test	underway	2 months	direct and calibrated measurement (± 2 μatm)	-3.0 ± 4.4	0 ± 2.9

Figure Captions:

Fig. 1 Schematic of the flow paths of the ProOceanus CO_2-Pro^{TM} pCO_2 sensor. See the text for details.

Fig. 2 The results of the ACT test in Kaneohe Bay: (A) the continuously hourly $pCO_{2,Pro}$ from the CO_2-Pro and the $pCO_{2,pHTA}$ calculated from discrete pH and TA; (B) the correlation between the δpCO_2 ($\delta pCO_2 = pCO_{2,Pro} - pCO_{2,pHTA}$) and $pCO_{2,Pro}$, the linear fit and the 95% prediction bands are shown; (C) δpCO_2 (8.4 ± 14.1 μatm) vs. time; (D) $\delta pCO_{2,corr} = pCO_{2,ProCorr} - pCO_{2,pHTA}$ (0 ± 7.4 μatm) vs. time, where $pCO_{2,ProCorr}$ is the sensor output corrected by $pCO_{2,pHTA}$ using the regression shown in panel B. Figure adapted from ACT (2009a).

Fig. 3 For the 12 Pacific transects during the SNOMS operation, (A) $\delta pCO_2 = pCO_{2,Pro} - pCO_{2,DICTA}$, where $pCO_{2,Pro}$ is the raw sensor output and $pCO_{2,DICTA}$ is calculated from DIC and TA, the mean and SD of δpCO_2 are 6.4 ± 12.3 μatm; (B) $\delta pCO_{2,corr} = pCO_{2,ProCorr} - pCO_{2,DICTA}$, where $pCO_{2,ProCorr}$ is the $pCO_{2,Pro}$ corrected by $pCO_{2,pHTA}$ for individual transects, the mean and SD of $\delta pCO_{2,corr}$ are 0.2 ± 7.8 μatm. The increasing δpCO_2 in transect 14 and the sudden changes in δpCO_2 in transect 17 are shown in panel (C) and (D), together with the $\delta pCO_{2,corr}$.

Fig. 4 (A) The overlapping route of the two ships of opportunity; the latitudinal distributions of (B) salinity, (C) SST, (D) pCO_2 measured by the PMEL and SNOMS systems; and their differences in (E) SST, salinity and (F) pCO_2. ΔTime is the difference in measuring time at the same location for the two ships.

Fig. 5 The differences of the simultaneous measurements (time difference less than 0.5 day and distance within 250 km) by the SNOMS and PMEL systems: (A) SST and salinity; (B) pCO_2.

Fig. 6 The variations of (A) temperature and salinity, (B) DIC and TA, (C) pCO_2 measured by the CO_2-Pro and the NOIZ system, (D) salinity normalized nDIC and nTA, (E) nitrate and phosphate, and (F) silicate and ammonia during the Aquatron test. The dashed line and the solid line correspond to the starting of the intercomparison and the substantial water top up event respectively. The arrow lines in panel (C) correspond to the starting of the bubbling of the CO_2-free gas. See the text for details.

Fig. 7 The results of the two-month intercomparison between the CO_2-Pro and the calibrated NOIZ system: (A) pCO_2; (B) the pCO_2 differences ($\delta pCO_2 = pCO_{2,Pro} - pCO_{2,NOIZ}$) vs. $pCO_{2,NOIZ}$, the linear fit and the 95% prediction bands are shown; (C) δpCO_2 vs. time; (D) $\delta pCO_{2,corr}$ is the pCO_2 differences between the corrected $pCO_{2,Pro}$ and $pCO_{2,NOIZ}$.

Fig. 8 (A) The concentrations of TA_{meas} from direct measurement and Alk_{sys} calculated from the measured DIC and pCO_2; (B) pCO_2 measured by the CO_2-Pro ($pCO_{2,Pro}$) and $pCO_{2,DICTA}$ calculated from the measured DIC and TA; (C) the differences of TA and pCO_2 between direct measurements and the carbonate calculations ($Alk_{excess} = TA_{meas} - Alk_{sys}$, $pCO_{2,bias} = pCO_{2,Pro} - pCO_{2,DICTA}$); (D) the correlation between the percentage of $pCO_{2,bias}$ and Alk_{excess} in comparison to the measured values ($\%pCO_{2,bias} = pCO_{2,bias} / pCO_{2,Pro}$, $\%Alk_{excess} = Alk_{excess} / TA_{meas}$).

Fig. 9 (A) A typical measuring cycle of the CO_2-Pro on PAP mooring, Δt_{cell} is the optical cell temperature deviation during the measurement in compared to that during the zero point calibration, $pCO_{2,raw}$ and $pCO_{2,tcorr}$ are the raw sensor outputs and those corrected for the influence of Δt_{cell}; (B) the errors in xCO_2 measurements resulting from Δt_{cell} for the three standard gases in the laboratory test, and those after correction for the temperature influence. See the text for details.

the laboratory test, and those after correction for the temperature influence. See the text for details.

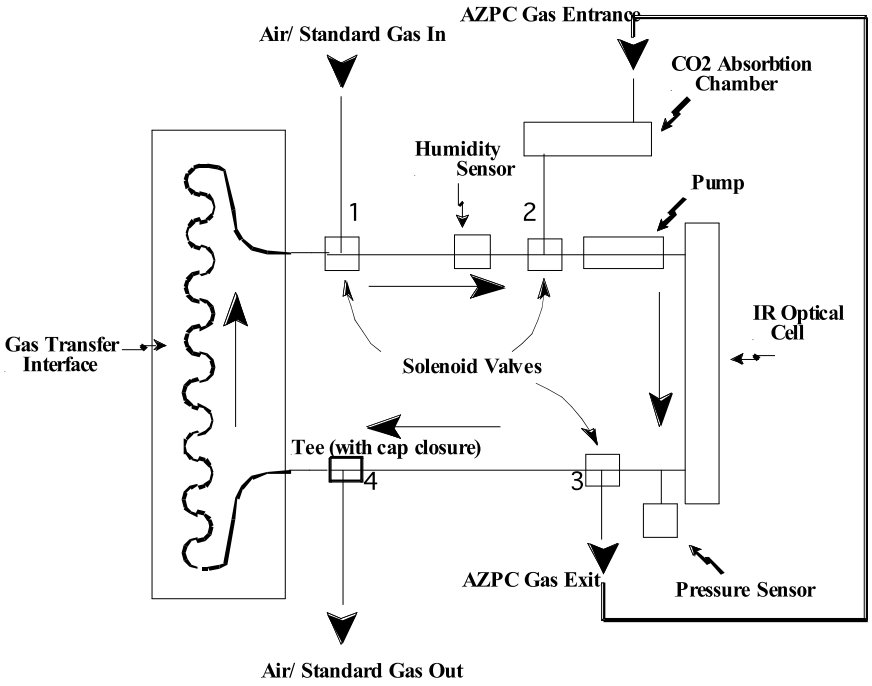

Fig. 1 Schematic of the flow paths of the ProOceanus CO_2-Pro^{TM} pCO_2 sensor. See the text for details.

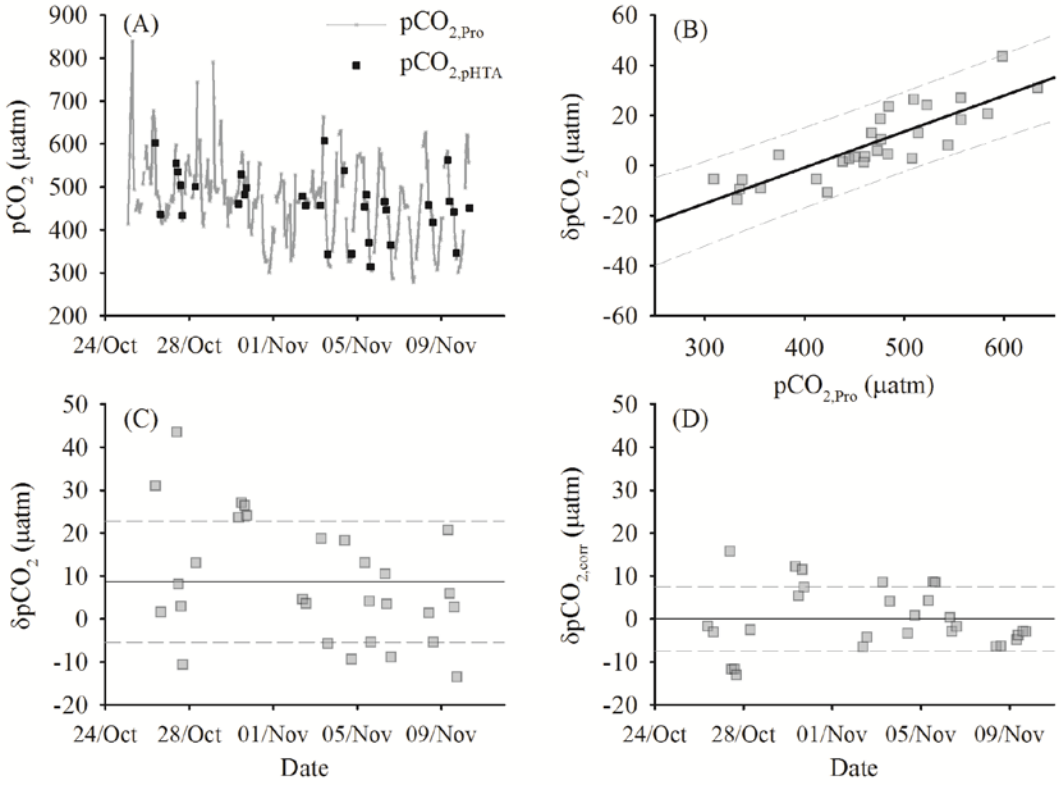

Fig. 2 The results of the ACT test in Kaneohe Bay: (A) the continuously hourly $pCO_{2,Pro}$ from the CO_2-Pro and the $pCO_{2,pHTA}$ calculated from discrete pH and TA; (B) the correlation between the δpCO_2 ($\delta pCO_2 = pCO_{2,Pro} - pCO_{2,pHTA}$) and $pCO_{2,Pro}$, the linear fit and the 95% prediction bands are shown; (C) δpCO_2 (8.4 ± 14.1 µatm) vs. time; (D) $\delta pCO_{2,corr} = pCO_{2,ProCorr} - pCO_{2,pHTA}$ (0 ± 7.4 µatm) vs. time, where $pCO_{2,ProCorr}$ is the sensor output corrected by $pCO_{2,pHTA}$ using the regression shown in panel B. Figure adapted from ACT (2009a).

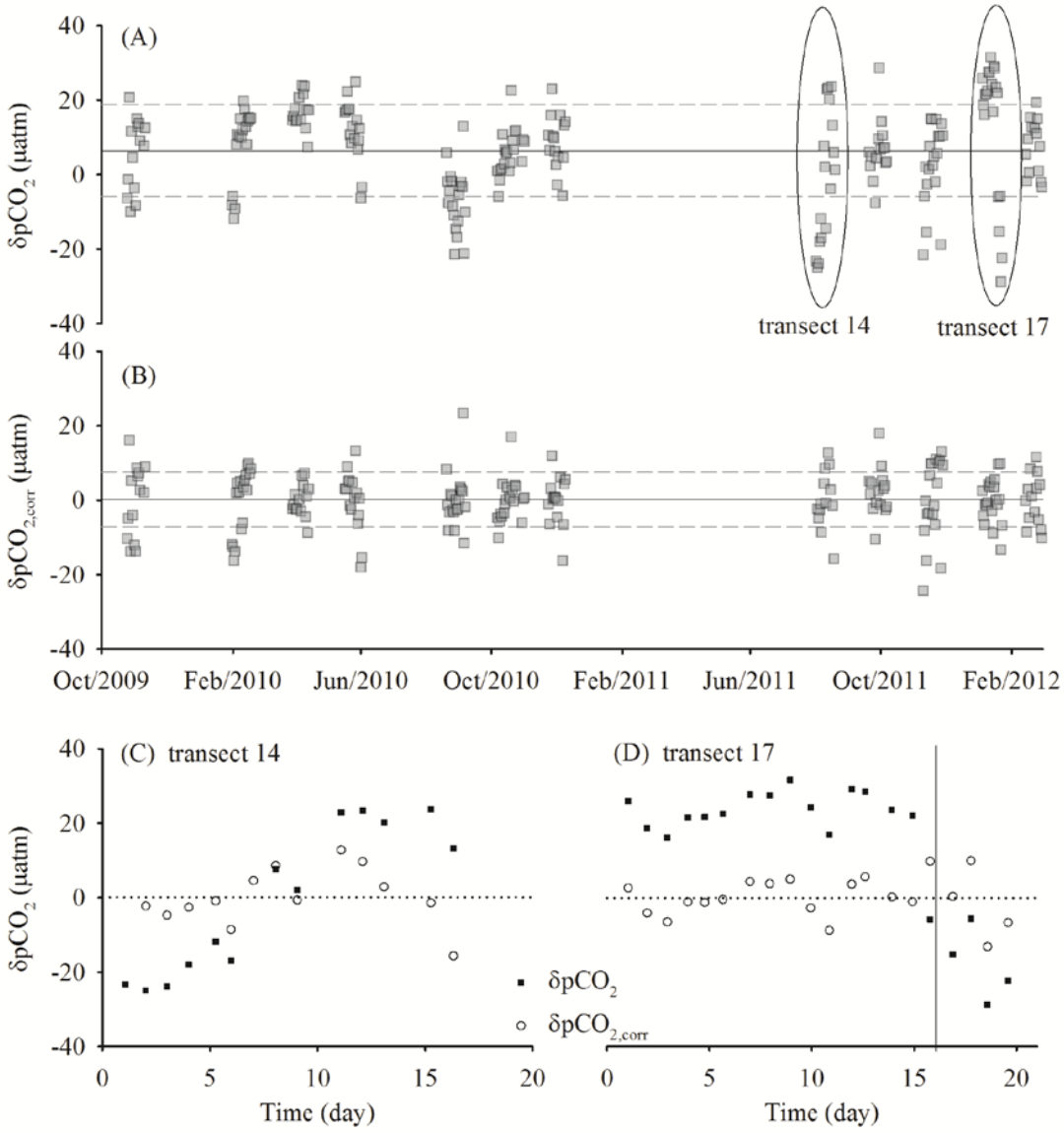

Fig. 3 For the 12 Pacific transects during the SNOMS operation, (A) $\delta pCO_2 = pCO_{2,Pro} - pCO_{2,DICTA}$, where $pCO_{2,Pro}$ is the raw sensor output and $pCO_{2,DICTA}$ is calculated from DIC and TA, the mean and SD of δpCO_2 are 6.4 ± 12.3 μatm; (B) $\delta pCO_{2,corr} = pCO_{2,ProCorr} - pCO_{2,DICTA}$, where $pCO_{2,ProCorr}$ is the $pCO_{2,Pro}$ corrected by $pCO_{2,pHTA}$ for individual transects, the mean and SD of $\delta pCO_{2,corr}$ are 0.2 ± 7.8 μatm. The increasing δpCO_2 in transect 14 and the sudden changes in δpCO_2 in transect 17 are shown in panel (C) and (D), together with the $\delta pCO_{2,corr}$.

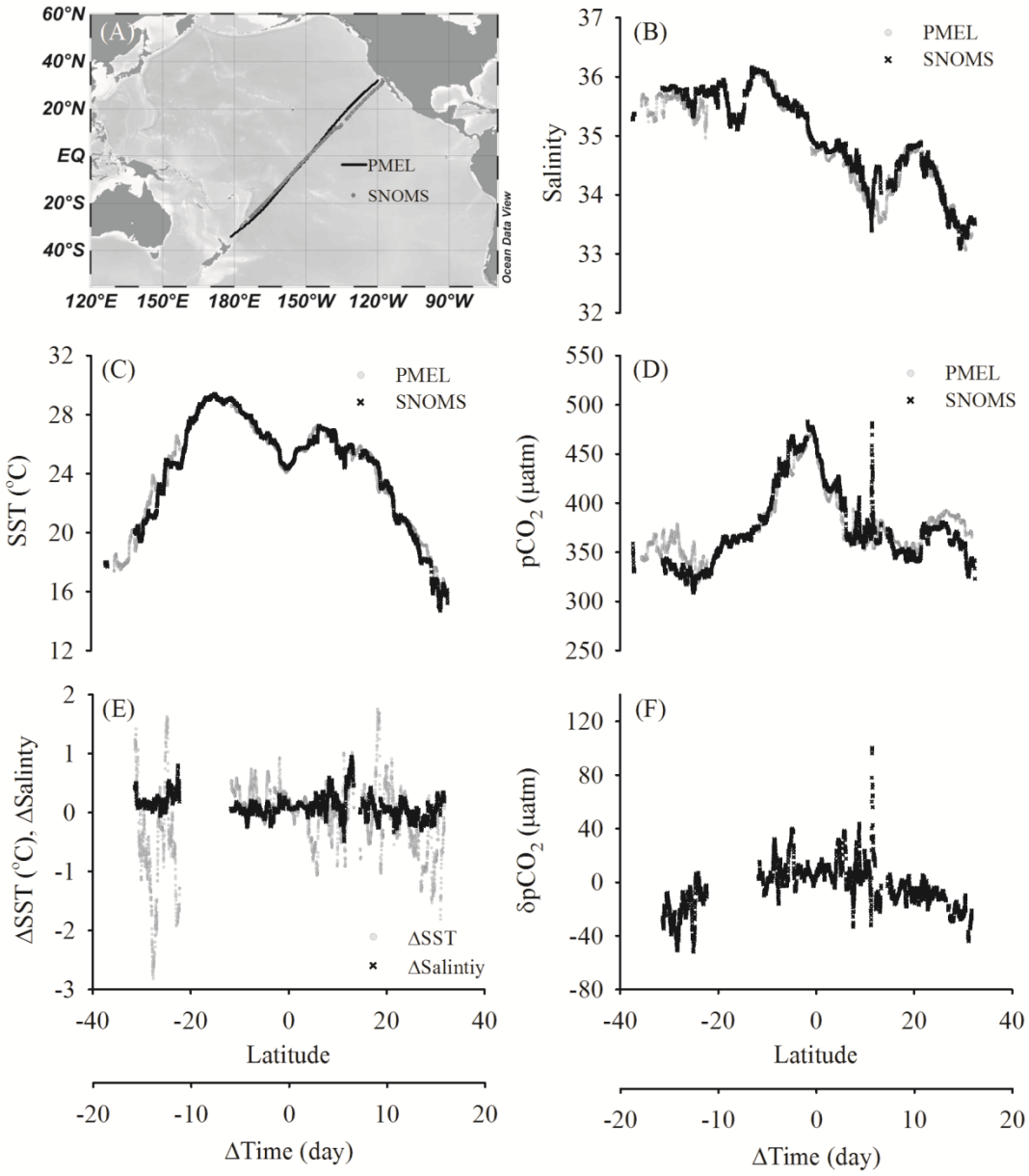

Fig. 4 (A) The overlapping route of the two ships of opportunity; the latitudinal distributions of (B) salinity, (C) SST, (D) pCO_2 measured by the PMEL and SNOMS systems; and their differences in (E) SST, salinity and (F) pCO_2. ΔTime is the difference in measuring time at the same location for the two ships.

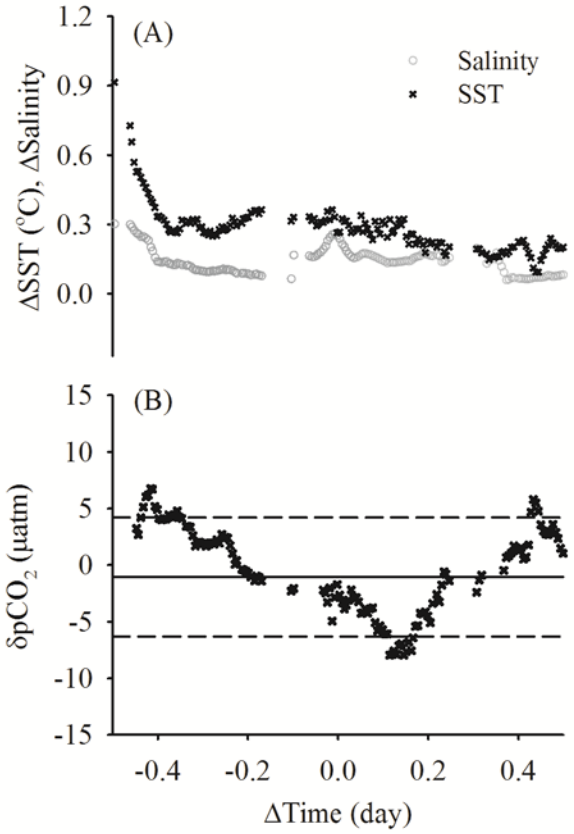

Fig. 5 The differences of the simultaneous measurements (time difference less than 0.5 day and distance within 250 km) by the SNOMS and PMEL systems: (A) SST and salinity; (B) pCO_2.

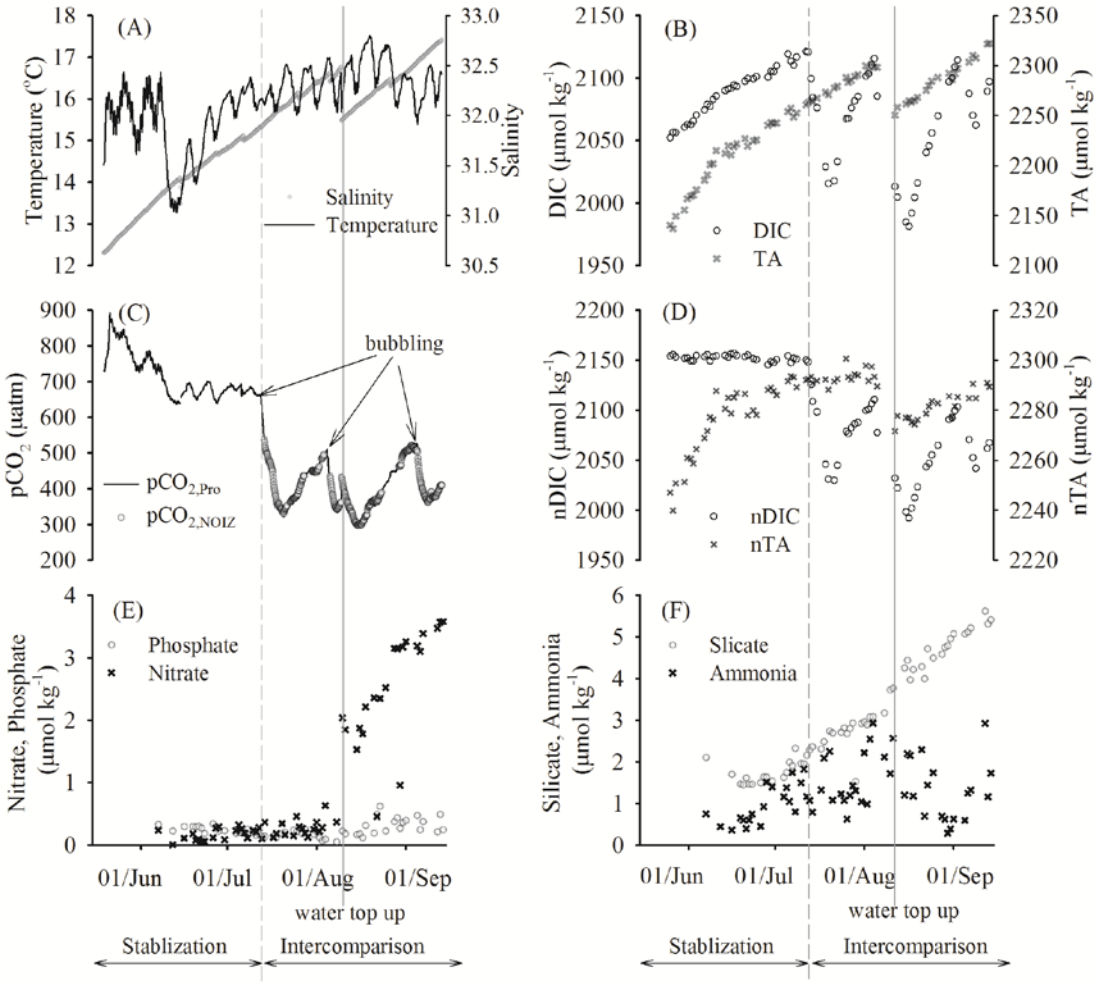

Fig. 6 The variations of (A) temperature and salinity, (B) DIC and TA, (C) pCO_2 measured by the CO_2-Pro and the NOIZ system, (D) salinity normalized nDIC and nTA, (E) nitrate and phosphate, and (F) silicate and ammonia during the Aquatron test. The dashed line and the solid line correspond to the starting of the intercomparison and the substantial water top up event respectively. The arrow lines in panel (C) correspond to the starting of the bubbling of the CO_2-free gas. See the text for details.

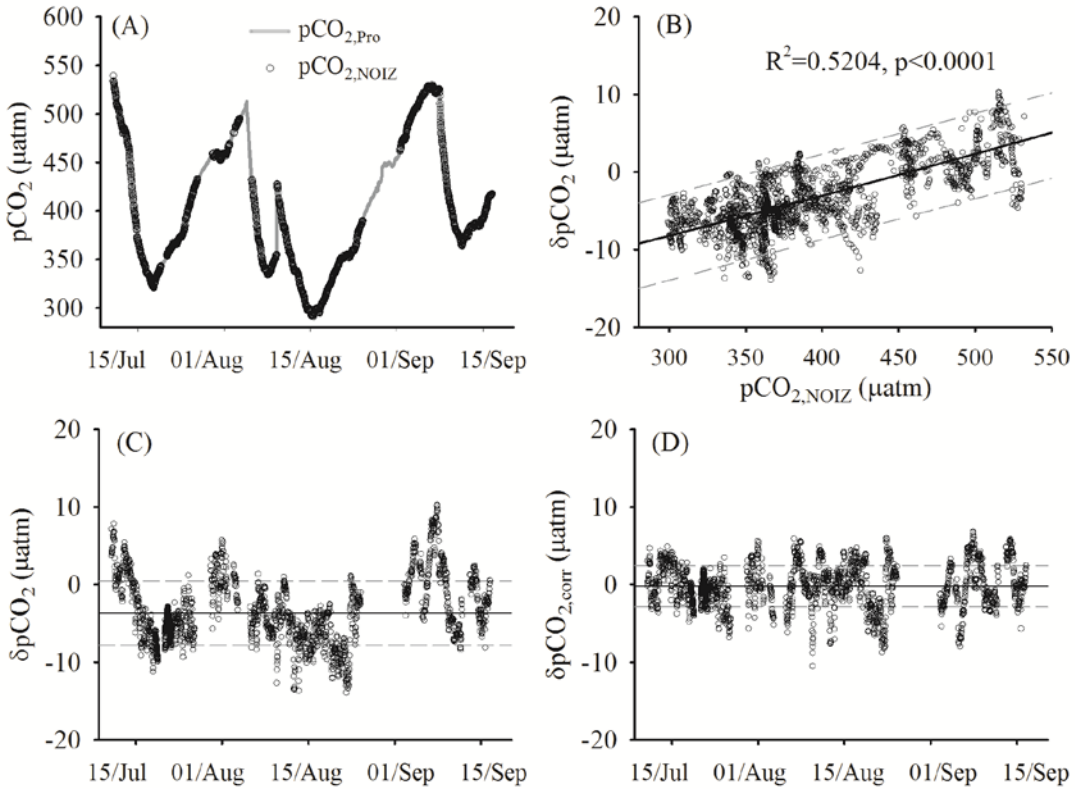

Fig. 7 The results of the two-month intercomparison between the CO_2-Pro and the calibrated NOIZ system: (A) pCO_2; (B) the pCO_2 differences ($\delta pCO_2 = pCO_{2,Pro} - pCO_{2,NOIZ}$) vs. $pCO_{2,NOIZ}$, the linear fit and the 95% prediction bands are shown; (C) δpCO_2 vs. time; (D) $\delta pCO_{2,corr}$ is the pCO_2 differences between the corrected $pCO_{2,Pro}$ and $pCO_{2,NOIZ}$.

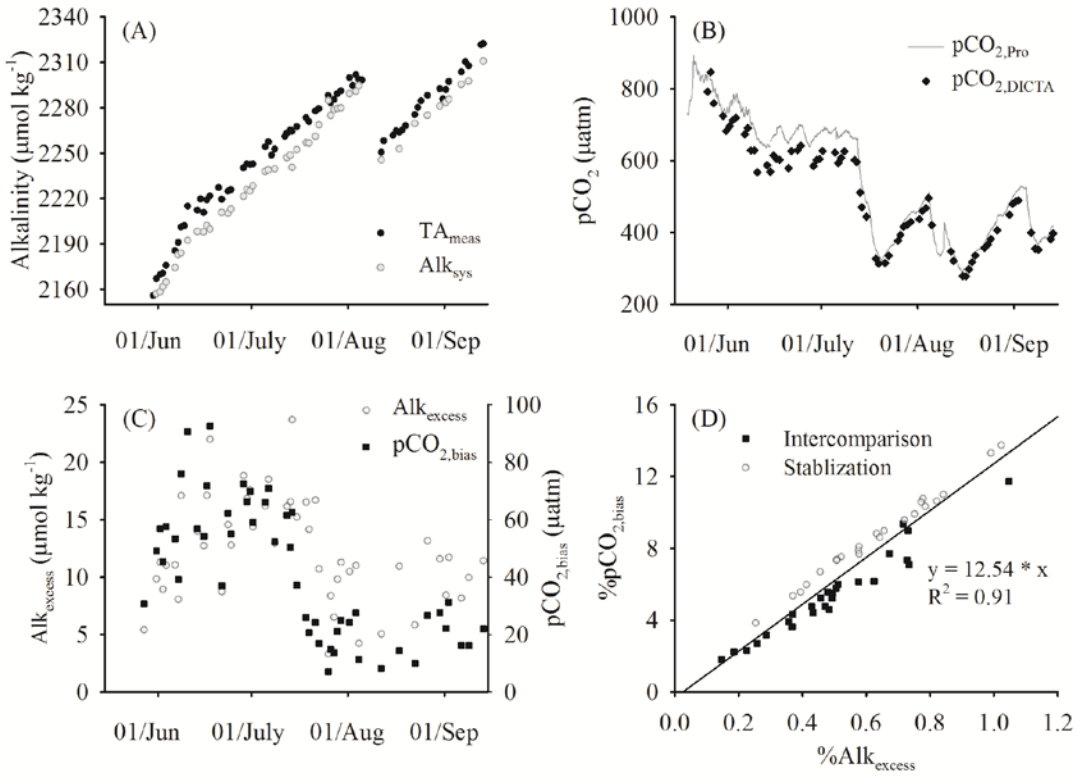

Fig. 8 (A) The concentrations of TA_{meas} from direct measurement and Alk_{sys} calculated from the measured DIC and pCO_2; (B) pCO_2 measured by the CO_2-Pro ($pCO_{2,Pro}$) and $pCO_{2,DICTA}$ calculated from the measured DIC and TA; (C) the differences of TA and pCO_2 between direct measurements and the carbonate calculations ($Alk_{excess} = TA_{meas} - Alk_{sys}$, $pCO_{2,bias} = pCO_{2,Pro} - pCO_{2,DICTA}$); (D) the correlation between the percentage of $pCO_{2,bias}$ and Alk_{excess} in comparison to the measured values ($\%pCO_{2,bias} = pCO_{2,bias} / pCO_{2,Pro}$, $\%Alk_{excess} = Alk_{excess} / TA_{meas}$).

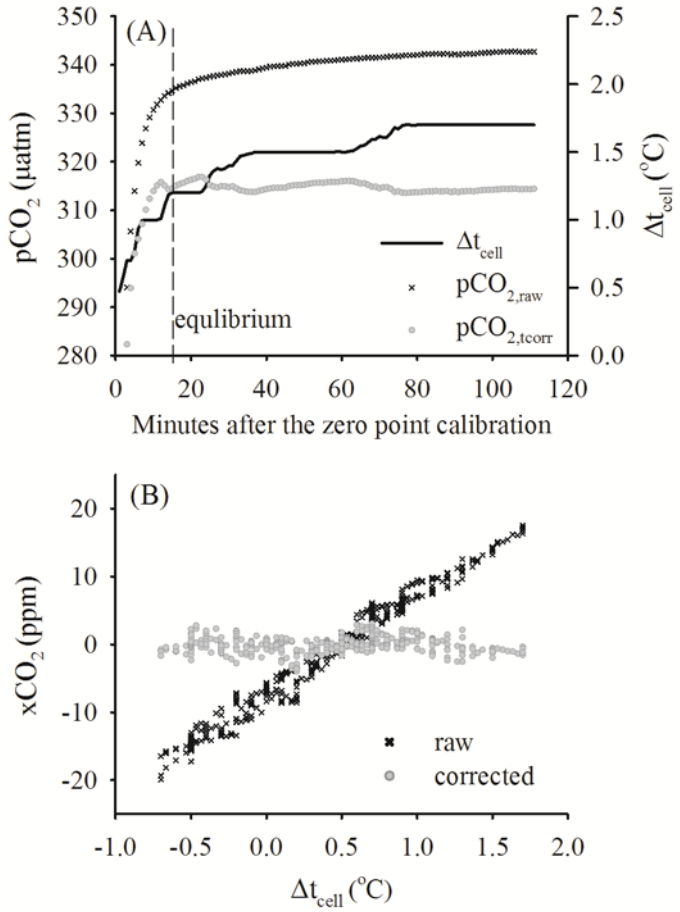

Fig. 9 (A) A typical measuring cycle of the CO_2-Pro on PAP mooring, Δt_{cell} is the optical cell temperature deviation during the measurement in compared to that during the zero point calibration, $pCO_{2,raw}$ and $pCO_{2,tcorr}$ are the raw sensor outputs and those corrected for the influence of Δt_{cell}; (B) the errors in xCO_2 measurements resulting from Δt_{cell} for the three standard gases in the laboratory test, and those after correction for the temperature influence. See the text for details.